To appear in the Astrophysical Journal (Part 1)

XMM-Newton and *VLA* Observations of the Variable Wolf-Rayet Star EZ CMa: Evidence for a Close Companion?

Stephen L. Skinner

CASA, Univ. of Colorado, Boulder, CO 80309-0389

Svetozar A. Zhekov

Space Research Institute, Moskovska str. 6, Sofia-1000, Bulgaria

Manuel Güdel

Paul Scherrer Institute, Würenlingen and Villigen, CH-5232 Switzerland

and

Werner Schmutz

Physikalisch-Meteorologisches Observatorium Davos, Dorfstrasse 33, CH-7260 Davos Dorf, Switzerland

ABSTRACT

We present new X-ray and radio observations of the Wolf-Rayet star EZ CMa (HD 50896) obtained with *XMM-Newton* and the *VLA*. This WN4 star exhibits optical and UV variability at a period of 3.765 d whose cause is unknown. Binarity may be responsible but the existence of a companion has not been proven. The radio spectral energy distribution of EZ CMa determined from *VLA* observations at five frequencies is in excellent agreement with predictions for free-free wind emission and the ionized mass-loss rate allowing for distance uncertainties is $\dot{M} = 3.8\ (\pm 2.6) \times 10^{-5}\ M_\odot\ yr^{-1}$. The CCD X-ray spectra show prominent Si XIII and S XV emission lines and can be acceptably modeled as an absorbed multi-temperature optically thin plasma, confirming earlier *ASCA* results. Nonsolar abundances are inferred with Fe notably deficient. The X-ray emission is dominated by cooler plasma at a temperature $kT_{cool} \approx 0.6$ keV, but a harder component is also detected and the derived temperature is $kT_{hot} \approx$ 3.0 - 4.2 keV if the emission is thermal. This is too high to be explained by radiative wind shock models and the X-ray luminosity of the hard component is three orders of magnitude lower than expected for accretion onto a neutron star companion. We show that the hard emission could be produced by the Wolf-Rayet wind shocking onto a normal (nondegenerate) stellar companion at close separation. Finally, using comparable data sets we demonstrate that the X-ray and radio properties of EZ CMa are strikingly similar to those of the WN5-6 star WR110. This similarity points to common X-ray and radio emission processes in WN stars and discredits the idea that EZ CMa is anomalous within its class.

Subject headings: radio continuum: stars — stars: individual (HD 50896) — stars: mass-loss — stars: winds — stars: Wolf-Rayet — X-rays: stars

1. Introduction

Theories of the origin of X-ray emission in massive stars are now being reexamined in light of new discoveries by the *XMM-Newton* and *Chandra* observatories. Traditionally, the X-ray emission of *single* OB and Wolf-Rayet (W-R) stars without companions has been attributed to shocks distributed throughout their winds that form as a result of line-driven flow instabilities (Lucy & White 1980; Lucy 1982; Baum et al. 1992; Gayley & Owocki 1995; Feldmeier et al. 1997; Owocki, Castor, & Rybicki 1988). Such emission is predicted to be relatively soft (kT $<$ 1 keV) and X-ray emission lines formed in an optically thick outflowing wind are expected to be blueshifted and asymmetric due to higher attenuation of the redward portion of the line by receding material on the far side of the star (MacFarlane

et al. 1991; Owocki & Cohen 2001).

Recently obtained X-ray grating spectra of several OB stars reveal properties that conflict with the predictions of traditional radiative wind shock theory. In particular, the emission lines of the O9 supergiant ζ Ori (Waldron & Cassinelli 2000) and the B0V star τ Sco (Cohen et al. 2002) are unshifted and show no obvious asymmetries. The lack of asymmetries is difficult to explain if the lines are indeed formed in shocked winds (Owocki & Cohen 2001). Also puzzling is the presence of narrow high-temperature Fe XXIII and Fe XXIV lines in τ Sco indicative of hot plasma well in excess of $\sim$1 keV. In contrast, much-needed support for the radiative wind shock paradigm has been received from *Chandra* and *XMM-Newton* grating observations of the O4 supergiant ζ Puppis, whose emission lines are blueshifted and asymmetric (Cassinelli et al. 2001; Kahn et al. 2001).

Although grating observations are providing stringent tests of wind shock theories in OB stars, the observational picture for W-R stars is much less complete due to the lack of suitable targets bright enough for X-ray grating observations. At current sensitivity levels, grating spectra of sufficient quality for emission line analysis can only be obtained for a few of the brightest W-R + OB binary systems such as γ^2 Velorum (Skinner et al. 2001; Dumm et al. 2002). Such binaries provide crucial information on extrastellar emission from colliding wind shocks between the stars (Cherepashchuk 1976; Prilutskii & Usov 1976; Usov 1992), but this emission is difficult to decouple from any intrinsic stellar emission that may be present since the binary components are usually not spatially resolved in X-rays.

We are thus undertaking an observing program using *XMM-Newton* aimed at acquiring moderate resolution CCD spectra of fainter W-R stars that are currently beyond the reach of gratings. These include high-interest objects such as the putatively single WN5-6 star WR 110 (Skinner et al. 2002, hereafter SZGS02) and possible binary systems such as EZ CMa discussed here. The large effective area of *XMM-Newton* is particularly well-suited for obtaining good-quality CCD spectra of such fainter objects in reasonable exposure times. Although CCD spectra do not provide the detailed information on line widths and profiles that can only be obtained with gratings, they are capable of discerning stronger emission lines and provide meaningful constraints on X-ray absorption and the overall distribution of plasma with temperature. Such information is more than adequate to discriminate between the relatively cool emission (kT $<$ 1 keV) that is expected from filamentary shocks distributed throughout the wind and harder emission at several keV that is predicted for colliding wind binaries. As such, CCD spectra provide an ideal means for identifying candidate colliding wind binaries that may be amenable to study at higher spectral resolution with next-generation X-ray telescopes.

We present here new *XMM-Newton* and *VLA* observations of the nitrogen-type W-R

star EZ CMa (= HD 50896 = WR6). This WN4 star has been extensively studied at all wavelengths and shows optical and ultraviolet variability at a well-documented 3.765 day optical period, the origin of which is still not understood. Various explanations have been proposed including an as yet undetected companion (Firmani et al. 1980; Lamontagne, Moffat & Lamarre 1986; Georgiev et al. 1999) and a rotationally modulated wind (St.-Louis et al. 1995). The *XMM-Newton* observations provide broader energy coverage and higher signal-to-noise (S/N) spectra than in previous observations, giving more accurate measurements of the X-ray absorption and plasma temperature distribution for comparison with emission models. The *VLA* data yield the first reliable determination of the radio spectral index based on single-epoch multifrequency data.

2. Previous X-ray and Radio Observations

EZ CMa has been observed in X-rays by *Einstein* (Moffat et al. 1982; White & Long 1986), *ROSAT* (Willis & Stevens 1996 = WS96), and *ASCA* (Skinner, Itoh, & Nagase 1997). The *Einstein* and *ROSAT* observations showed day-to-day X-ray variability at levels of $\leq$30% but the reality of short-term ($\leq$ 1 hour) variability reported by White & Long has been questioned in subsequent work (WS96). Moffat et al. claimed that weak modulation at the 3.76 d optical period was present in *Einstein* data , but a sequence of eight *ROSAT* exposures failed to confirm this (WS96). Low signal-to-noise *ASCA* spectra revealed weak emission lines (Si XIII and S XV) and provided the first clear evidence that the X-ray emission is due to an absorbed multi-temperature optically thin plasma. The *ASCA* observation was not sensitive enough to detect any photons above $\sim$5 keV, but the more sensitive *XMM-Newton* observation discussed here shows that such emission is present.

At radio frequencies Hogg (1989) obtained an average 6 cm flux density $S_{4.89}$ = 1.05 $\pm$ 0.08 mJy from four VLA observations spanning 3.3 years, with no significant variability. Contreras & Rodriquez (2000) analyzed four deep 3.6 cm VLA observations in both A and D configurations obtained during a $\approx$6 month interval. The source was unresolved and flux densities in the range $S_{8.44}$ = 1.38 $\pm$ 0.03 to 1.62 $\pm$ 0.03 mJy were obtained. Given the small flux uncertainties, their results could signal episodic variability. Higher frequency measurements were made by Altenhoff et al. (1994) at 250 GHz, obtaining S_{250} = 17 $\pm$ 3 mJy. A 230 GHz SEST observation by Leitherer & Robert (1991) gave S_{230} = 14.1 $\pm$ 3.1 mJy.

3. Observations

3.1. XMM-Newton Observations

XMM-Newton observed EZ CMa on 29 - 30 October 2001 as summarized in Table 1. The X-ray telescope is described by Jansen et al. (2001) and our analysis focuses on CCD imaging spectroscopy with the European Photon Imaging Camera (EPIC). Data were obtained simultaneously with the EPIC-PN camera (Strüder et al. 2001) and two identical EPIC-MOS cameras (MOS-1 and MOS-2; Turner et al. 2001). We used full-window mode and the thick optical blocking filter. The PN and MOS cameras provide a $\approx 30'$ diameter field-of-view and energy coverage from ≈0.2 - 15 keV, moderate energy resolution ($E/\Delta E \approx$ 20 - 50), and $\approx 5''$ FWHM angular resolution. Grating spectrometer data were also acquired but lacked sufficient counts for analysis.

Data reduction followed standard procedures using the *XMM-Newton* Science Analysis System software (SAS vers. 5.2). Pipeline-processed events files generated using the most current calibration data were filtered with EVSELECT to select good event patterns. Spectra and light curves were extracted from the filtered events lists within circular regions centered on EZ CMa of radii $\approx 40''$ (PN) and $\approx 52''$ (MOS). The PN extraction radius was limited to $\approx 40''$ in order to exclude photons from an adjacent CCD, thus minimizing calibration uncertainties. The $\approx 52''$ extraction radius for MOS excludes a weak field source lying $\approx 57''$ to the south (Fig. 1). Background was extracted from source-free regions of the same size on the same CCD as the source. Spectra were rebinned to a minimum of 20 counts per bin for analysis with XSPEC vers. 11.1 (Arnaud 1996) using various models. These included discrete temperature optically thin plasma codes (VAPEC and VMEKAL) and the differential emission measure (DEM) model C6PVMKL, which is an iterative algorithm based on Chebyshev polynomials (Lemen et al. 1989). For the hard component, bremsstrahlung and power-law models were also examined. All models included an absorption component based on Morrison & McCammon (1983) cross sections.

3.2. VLA Observations

EZ CMa was observed with the NRAO [1] VLA during a 3.5 hour interval on 1999 Oct. 19 with the array in hybrid BnA configuration, as summarized in Table 2. It was observed and detected at five frequencies: 1.42 GHz (21 cm), 4.86 GHz (6 cm), 8.44 GHz (3.6 cm),

[1]The National Radio Astronomy Observatory (NRAO) is a facility of the National Science Foundation operated under cooperative agreement by Associated Universities Inc.

14.94 GHz (2 cm), and 22.46 GHz (1.3 cm). The observations were made with the full array (minus two inoperable antennas) at each frequency in scans of ≈10 - 12 minutes duration interleaved with scans of the phase calibrator 0608−223. The primary flux calibrator 3C286 was observed at each frequency.

Data were edited and calibrated using the AIPS [2] software package. Maps were produced in both total intensity (Stokes I) and circularly polarized intensity (Stokes V) using the AIPS task IMAGR with natural weighting. Both peak and total (integrated) fluxes were measured in cleaned maps using the AIPS tasks TVSTAT (pixel summation within a region defined by the 2σ contour) and IMFIT (Gaussian source model). These two methods gave good agreement, differing by no more than the RMS noise in the image.

4. Results

4.1. X-ray Properties of EZ CMa

We summarize below the main observational results from analysis of the images, light curves, and CCD spectra.

4.1.1. X-ray Images

Figure 1 shows the inner region of the combined MOS1 and MOS2 images in broad-band (0.3 - 10 keV) and hard-band (5 - 10 keV) energy filters. EZ CMa is clearly detected in both bands and the X-ray position in Table 3 is offset by only 0.″59 from the *Hipparcos* optical position (Perryman et al. 1997). A weak field source lying 57.4″ south of EZ CMa is visible but there is no SIMBAD counterpart within 30″ of this faint source.

The hard-band emission is also seen in the PN image, which shows 41 net counts (S/N = 5.8) in the 5 - 10 keV range. Thus, the hard-band emission is present in all three detectors and comprises ≈1.5% of the total counts in each detector. The hard-band emission is not extended and the hard emission peak lies within 0.″6 of the EZ CMa *Hipparcos* position. This is the first detection of X-ray photons above 5 keV in EZ CMa and is attributable to the larger effective area of *XMM-Newton*.

[2]Astronomical Image Processing System (AIPS) is a software package developed by NRAO.

4.1.2. X-ray Light Curves

Figure 2 shows the MOS-1 and MOS-2 light curves in the 0.3 - 8 keV range. This restricted energy range reduces background and thus improves sensitivity to any real variability. The average count rate in each MOS is 0.12 ± 0.02 ($\pm 1\sigma$) counts s^{-1}. There are no MOS fluctuations greater than $\pm 2.1\sigma$ and there is no clear correspondence between the largest fluctuations in one detector and the other. A fit of an assumed constant count rate source to each light curve binned at 512 s gives P(const) = 0.92 (χ^2/dof = 13.4/22) for MOS-1 and P(const) = 0.87 (χ^2/dof = 15.5/23) for MOS-2. Reducing the bin size to 256 s gives nearly identical values P(const) = 0.92 and 0.86 for MOS-1 and MOS-2.

By comparison, the PN light curve has an average count rate of 0.26 ± 0.03 counts s^{-1}. At a binsize of 256 s there are no fluctuations greater than $\pm 2.2\sigma$ and a constant count rate fit gives P(const) = 0.62 (χ^2/dof = 32.9/36). Light curves in soft and hard-bands were also generated and showed similar statistics. For example, the PN light curve in the 2.5 - 8.0 keV band gave P(const) = 0.78 (χ^2/dof = 4.75/8) when binned at 800 s intervals (≈20 cts/bin).

In summary, we find no large amplitude ($\geq 3\sigma$) variability during the 3.4 hour observation, but lower level fluctuations at the $\pm 2\sigma$ level are present. The probability that these fluctuations represent real variability is P(var) = 0.08 - 0.13 in MOS and P(var) = 0.38 in PN. Thus, real low-level variability is not totally ruled out but is considered unlikely.

A comparison of *XMM-Newton* and *ASCA* fluxes does suggest that longer term variability is present. The observed (absorbed) flux in the 0.5 - 10 keV range measured by *ASCA* in October 1995 was F_x(0.5 - 10 keV) = 1.26×10^{-12} ergs cm^{-2} s^{-1} (Skinner, Itoh, & Nagase 1997). In this same energy range the flux observed by *XMM-Newton* is F_x(0.5 - 10 keV) = 0.96×10^{-12} ergs cm^{-2} s^{-1}. This represents a 24% decrease, some of which could be due to absolute flux calibration differences between *XMM-Newton* and *ASCA*. Thus, any real variability is within the day-to-day fluctuation range of ≤30% found in previous *ROSAT* monitoring (WS96).

4.1.3. X-ray Spectra

The EPIC-PN spectrum is shown in Figure 3. Several emission lines are visible including Mg XI (log T_{max} = 6.8), Si XIII (log T_{max} = 7.0), S XV (log T_{max} = 7.2) and possible Fe lines in the crowded region near 1 keV. The Si and S lines confirm earlier detections in *ASCA* spectra (Fig. 3 of Skinner, Itoh, & Nagase 1997).

Based on a comparison of several models fitted to all three spectra simultaneously,

we conclude that the best fit is obtained with an absorbed two-temperature optically thin plasma model (2T VAPEC) using nonsolar abundances (Sec. 4.1.4). Isothermal models are unacceptable. The best-fit parameters for the 2T VAPEC model are given in Table 3, and an overlay of this model on the MOS1 spectrum is shown in Figure 4. The emission measure is dominated by a cool component at $kT_{cool} \approx 0.6$ keV, but hotter emission is also present. Assuming that the hotter emission is thermal, its derived temperature is $kT_{hot} = 3.5$ [3.0 - 4.2] keV, where brackets enclose the 90% confidence interval. About one-half of the observed (absorbed) flux is due to the hot component (Table 3). As shown in Figure 5, essentially all of the flux above 2.5 keV is due to the hot component. For comparison, we have also fitted the *ASCA* SIS0 spectrum obtained in October 1995 with the 2T VAPEC model. Very similar results were obtained and the best-fit values of N_H, kT_{cool}, and kT_{hot} all lie within the 90% confindence ranges determined from *XMM-Newton* spectra (Table 3).

Because of the rather high temperature of the hot component and the low S/N ratio above 4 keV, the hot component can also be modeled as bremsstrahlung or a power-law. Replacing the hot optically thin plasma component in the 2T VAPEC model with a BREMSS model in XSPEC gives $kT_{brem} = 3.4$ [3.0 - 4.1] keV and no change in the reduced χ^2. Thus, a bremsstrahlung model for the hard component is essentially identical to an optically thin plasma model as expected at these higher temperatures. If a power-law model with an energy dependence E^{-q} is used for the hot component then the best-fit photon power-law index is $q = 2.5$ and the reduced χ^2 increases by 1.6% over the 2T VAPEC value. Issues related to power-law models were discussed in SZGS02 and also apply here.

The presence of a cool and hot emission component is confirmed in the emission measure distribution derived from a fit to all three spectra with the C6PVMKL model, as shown in Figure 6. The cool DEM component has a maximum contribution at $kT_{cool} \approx 0.55$ keV, in good agreement with 2T models. The DEM also shows a turnup above ∼4 keV signalling hotter plasma. However, the precise temperature of the hot component cannot be reliably determined from DEM models due to low signal-to-noise above 4 keV.

Some soft emission below 0.5 keV appears to be present in the PN spectrum (Fig. 3), but is not as obvious in the MOS spectra (Fig. 4). PN images in the soft 0.2 - 0.5 keV range show unresolved emission at the stellar position but there is no indication of extended emission from the surrounding ring nebula S 308, in agreement with *ROSAT* findings (WS96). The best-fit 2T VAPEC model (Table 3) with a single absorption component at $N_H = 4 \times 10^{21}$ cm^{-2} underestimates the flux in the PN spectrum by about 20% (-1.8σ) in the 0.3 - 0.43 keV range (see also Fig. 4 of WS96). However, this model provides a satisfactory MOS fit at 0.4 keV. The soft residual in the PN fit can be removed by adding a third optically thin plasma component to the 2T VAPEC model at an uncertain temperature $kT_{soft} < 0.3$ keV

viewed under low (≈interstellar) absorption N_H(ISM) ≈ 5 × 10^{20} cm^{-2}. Thus, there could be a contribution at low energies from very soft emission which would most likely originate far out in the wind. But, we are unable to state with confidence that such very soft emission is present because of PN calibration uncertainties below 0.5 keV and the reduced sensitivity to soft emission that results from use of the thick optical blocking filter.

4.1.4. Abundances

We are unable to obtain satisfactory spectral fits using either solar abundances (Anders & Grevesse 1989, hereafter AG89) or the WN abundances given in Table 1 of van der Hucht, Cassinelli, & Williams 1986 (VCW86). An absorbed 2T VAPEC model using solar abundances gives χ^2/dof = 465.5/223 = 2.09 and the same model with WN abundances gives χ^2/dof = 383.4/223 = 1.72. Although neither fit is acceptable, the WN abundances yield somewhat better results and we have thus used them as our reference for further variable abundance fitting. These canonical WN abundances reflect chemical composition changes that are thought to occur in WN stars as a result of advanced nucleosynthesis including hydrogen depletion and the enhancment of helium and nitrogen (Willis 1996).

The spectral fits are significantly improved by allowing the abundances of N, Ne, Mg, Si, S, and Fe to vary relative to the VCW86 values. Also, the fit to the weak feature near 3.15 keV can be improved by adding Ar to the canonical WN abundance table and letting it vary. This weak feature could be Ar XVII, but the S XVI line at 3.11 keV may also be contributing. A comparison of 2T VAPEC and C6PVMKL models suggests that Fe is underabundant in EZ CMa by about a factor of four relative to the values in VCW86 (even when Ne is also allowed to vary) and that S is overabundant. Specifically, 2T VAPEC fits give Fe = 0.23 [0.15 - 0.32] and S = 2.0 [1.4 - 2.9] relative to the VCW86 values, which are by number: Fe/H = 1.904 × 10^{-3} and S/H = 7.600 × 10^{-4}. Similar values are obtained with a 2T VMEKAL optically thin plasma model. If cosmic abundances (AG89) are used as a reference then the underabundance of Fe persists.

4.1.5. Absorption and A_v

Acceptable fits give an equivalent neutral hydrogen column density N_H = 4.0 [3.4 - 4.4] × 10^{21} cm^{-2}. This value corresponds to a visual extinction A_v = 1.8 [1.5 - 2] using the conversion of Gorenstein (1975), which is at least twice as large as the values A_v = 0.00

- 0.82 determined from optical studies (van der Hucht 2001, hereafter vdH01). However, if we adopt an absolute visual magnitude $M_v = -3.5$ as typical for WN4 stars (Fig. 4 of vdH01), $v = 6.94$ (vdh01) and the *Hipparcos* distance of 575 pc, then we obtain $A_v = 1.64$, which is in good agreement with the value obtained above from the X-ray spectra. Thus, the larger A_v determined from X-ray spectra is not unrealistic but two factors should be kept in mind. First, a typical value of M_v is difficult to define for WN stars since there is no definite relation between spectral type and bolometric luminosity. Second, the *Hipparcos* distance is quite uncertain as evident from the parallax measurement $\pi = 1.74 \pm 0.76$ mas (Perryman et al. 1997).

4.2. Radio Properties

The VLA position (Table 2) is in excellent agreement with the Hipparcos position, with a radio − optical offset ΔRA = +0.001 s and ΔDEC = +0.07″. The source is unresolved down to the smallest synthesized beamsize of 0.″4 × 0.″3 as indicated by the good agreement between the peak and total fluxes. The total flux at 4.86 GHz is nearly identical to the value $S_{4.86} = 1.05 \pm 0.08$ mJy measured in 1980 - 1983 with the VLA (Hogg 1989). No circular polarization was detected and the most stringent upper limit on the fractional circular polarization (π_c) from the 8.44 GHz Stokes V image is $\pi_c \leq 0.067$ (3σ).

As shown in Figure 6, the total fluxes are well-approximated by a power-law of the form $S_\nu \propto \nu^\alpha$, where $\alpha = +0.69 \pm 0.05$ (90% confidence errors). This spectral index agrees very well with that expected for free-free emission from a spherical ionized constant-velocity wind (Wright & Barlow 1975). It is also consistent with the value $\alpha = +0.64 \pm 0.06$ derived by Leitherer & Robert (1991) using non-contemporaneous flux measurements. Extrapolating the total 22.4 GHz flux to 250 GHz using $\alpha = +0.69$ gives a predicted value $S_{250}^{(pred)} = 16.6 \pm 0.8$ mJy, which is consistent with the measurement $S_{250} = 17 \pm 3$ mJy obtained by Altenhoff, Thum, & Wendker (1994). Thus, there is good reason to believe that the $\alpha = +0.69$ power-law extends to frequencies an order of magnitude higher than observed here with the VLA.

4.2.1. Mass Loss Rate

The ionized mass loss rate for an assumed constant-velocity wind can be estimated using the result of Wright & Barlow (1975), namely $\dot{M} = C_0 v_\infty S_\nu^{0.75} d_{kpc}^{1.5}$ $M_\odot$ yr^{-1}, where $C_0 = 0.095\mu/[Z\sqrt{\gamma g \nu}]$. Here, v_∞ (km s^{-1}) is the terminal wind speed, S_ν (Jy) is the observed

radio flux at frequency ν (Hz), d_{kpc} (kpc) is the stellar distance, μ is the mean atomic weight per nucleon, Z is the rms ionic charge, γ is the mean number of free electrons per nucleon, and g is the free-free Gaunt factor. To evaluate this expression we use the highest signal-to-noise radio detection at $\nu = 8.44$ GHz, $S_{8.44} = 1.74$ mJy (Table 2), $v_\infty = 1700$ km s^{-1} (Hillier 1987; Prinja, Barlow, and Howarth 1990), Z = 1, $\gamma = 1$, and g = 4.78 at 8.44 GHz from the approximation for the free-free Gaunt factor given in Eq. [8] of Abbott et al. (1986), assuming a temperature at the radio photosphere of T = 10000 K (VCW86). These values give $\dot{M} = 6.85 \times 10^{-6}\ \mu\ d_{kpc}^{1.5}\ M_\odot\ yr^{-1}$. Assuming $\mu = 3.9$ for a WN star (VCW86) this becomes $\dot{M} = 2.67 \times 10^{-5} d_{kpc}^{1.5}\ M_\odot\ yr^{-1}$. The wind luminosity is $L_{wind} = (1/2)\dot{M}v_\infty^2 = 2.4 \times 10^{37} d_{kpc}^{1.5}$ ergs s^{-1}.

Using the range of distance estimates from the Hipparcos value of 0.575 kpc to 1.8 kpc from Howarth & Schmutz (1995) to evaluate the above quantities we obtain $\dot{M} = (1.2 - 6.4) \times 10^{-5}\ M_\odot\ yr^{-1}$ and $L_{wind} = (1.1 - 5.9) \times 10^{37}$ ergs s^{-1}. Smaller values of $\dot{M}$ are obtained using values of Z > 1 and $\gamma > 1$ obtained from specific atmospheric models (VCW86). However, the values of Z and γ are quite sensitive to poorly-known stellar parameters and we have thus adopted Z = 1 and $\gamma = 1$ in the above calculation.

5. Discussion

The new observational results discussed above provide the most detailed picture to date of the X-ray and centimeter radio properties of EZ CMa. Below, we make comparisons with previous studies and comment on specific emission models.

5.1. WN Stars: Comparative Spectroscopy

The *XMM-Newton* and VLA data for EZ CMa provide a good basis for comparison with similar data recently obtained for WR 110 (SZGS02). For the first time we are able to directly compare the X-ray and radio properties of two WN stars having similar spectral types using analogous data sets.

Table 4 summarizes the X-ray and radio properties of EZ CMa and WR 110, and their X-ray spectra are compared in Figure 8. Overall, the two stars are strikingly similar and the same physical processes are very likely responsible for the X-rays and radio emission in both stars. One notable difference is the larger N_H for WR 110, attributable to its stronger interstellar absorption toward the Galactic center (SZGS02). The uncertain distance for EZ CMa introduces some ambiguity into the calculation of $\dot{M}$ and L_x. But, as Table 4 shows, if

an intermediate distance of 1.2 kpc is adopted for EZ CMa then $\dot{M}$ and L_x agree with WR 110 to better than a factor of two.

5.2. Radiative Wind Shocks

The *XMM-Newton* spectra provide some constraints on wind shock models. The dominant cool emission component peaking near $kT_{cool} \approx 0.6$ keV can potentially be explained by radiative wind shock models, but the hot component requires a different explanation.

Assuming that the cool component is due to shocks distributed throughout the wind, then the observed X-ray temperature provides constraints on the shock speed v_s using the adiabatic shock formula $kT_s = (3/16)\bar{m}v_s^2$. For a helium-rich WN wind $\bar{m} = (4/3)m_p$ where m_p is the proton mass. The value $kT_{cool} \approx 0.6$ keV gives a typical shock speed $v_s \approx 480$ km s^{-1} but the range in temperatures of ≈0.3 - 0.8 keV inferred from the FWHM of the DEM model implies a range of shock speeds $v_s \approx 340$ - 550 km s^{-1}. These values overlap the range of shock velocity jumps $\Delta v = 500$ - 1000 km s^{-1} derived in numerical simulations of radiatively driven winds (Owocki et al. 1988).

The average filling factor f of X-ray emitting plasma in the wind can be estimated using the procedure given in SZGS02 and the mass-loss parameters from Section 4.2.1. We define $f = EM_x/EM_{tot}$ where EM_x is the volume emission measure of the X-ray emitting plasma and EM_{tot} is the total volume emission measure in the wind. For a He-dominated wind we obtain $f = 5.34 \times 10^{-3}(R_*/R_\odot)norm/d_{kpc}$, where *norm* is the normalization factor from XSPEC VAPEC models. Since only the cool X-ray component can be attributed to radiative wind shocks, we set $norm = norm_{cool}$ from Table 3 and obtain $f = 1.8 \times 10^{-7}(R_*/R_\odot)/d_{kpc}$. For radii of a few solar radii (Hillier 1987) and the range of estimated distances 0.58 - 1.8 kpc, the filling factor need not be larger than $f \sim 10^{-6}$.

The emergent cool emission detected by *XMM-Newton* must originate at large distances from the star unless the wind is clumped. Using the same procedure as in SZGS02 along with an intermediate distance d = 1.2 kpc and the mass loss parameters in Sec. 4.2.1, the radius of optical depth unity at 1 keV is $R_{\tau=1}(E = 1\ keV) = 1.58 \times 10^{14}$ cm ≈ 10.6 AU. Assuming $R_* \approx 2\ R_\odot$ as a representative value (Hillier 1987; Hamann & Koesterke 1998), then $R_{\tau=1}(E = 1\ keV) \approx 1130\ R_*$. The harder emission could be coming from much smaller radii. Specifically, $R_{\tau=1}(E = 4\ keV) \approx 0.3$ AU assuming that the wind absorption cross-section for X-rays σ_w scales with energy according to $\sigma_w \propto E^{-2.5}$ (Fig. 1 of Ignace, Oskinova, & Foullon 2000).

The shock speeds, filling factor and value of $R_{\tau=1}(E = 1\ keV)$ computed above are

nearly identical to those derived previously for WR 110 (SZGS02). The unit optical depth calculations for EZ CMa and WR 110 suggest that soft X-rays ($\sim$1 keV) emerge at many hundreds of stellar radii in WR stars assuming homogeneous winds, but smaller emergent radii would be possible for clumped winds. Similar conclusions have been reached for some O-type stars (e.g. Hillier et al. 1993). Detailed hydrodynamic simulations are now needed to determine if instability-generated wind shocks can persist to hundreds of radii in WR stars, analogous to those recently undertaken for OB stars by Runacres & Owocki (2002).

5.3. On the Possibility of a Compact Companion

Binarity has been suggested as one possible means of explaining the 3.765 day optical variability of EZ CMa. An estimate of the mass of the putative companion M_{comp} = 1.3 ($\pm$0.4) $M_\odot$ derived by Firmani et al. (1980) raised speculation that EZ CMa could have a compact companion (c), making it a rare WR + c system (Lamontagne et al. 1986; White & Long1986). But, it was shown that the X-ray luminosity of EZ CMa is about three orders of magnitude lower than the accretion luminosity $L_x^{(acc)}$ $\sim 10^{36}$ ergs s^{-1} expected for accretion of the W-R wind onto a neutron star (Stevens & Willis 1998). Similar arguments against a black hole companion based on *ASCA* luminosities were given by Skinner et al. (1997).

The *XMM-Newton* results confirm the above luminosity deficit, giving an unabsorbed luminosity L_x = (0.2 - 10 keV) = $3.46 \times 10^{32} d_{kpc}^2$ ergs s^{-1}. At the upper end of current distance estimates, d = 1.8 kpc and $L_x = 10^{33.0}$ ergs s^{-1}. If only the contribution of the hard component is considered, then $L_{x,hard}$(0.2 - 10 keV) = $10^{32.5}$ ergs s^{-1}. Thus, if a neutron star companion is present then some mechanism such as rapid rotation near breakup (Davidson & Ostriker 1973) is needed to inhibit accretion.

The strong similarity between EZ CMa and WR 110 (Table 4) presents a new challenge for the compact companion hypothesis. WR 110 has so far shown no clear signs of binarity or periodic optical variability and has not previously been proposed as a candidate WR + c system. If EZ CMa has a compact companion, then it is not clear why its X-ray and radio properties would so closely mimic those of another WN star for which evidence of a compact companion is lacking.

5.4. On the Possibility of a Normal Stellar Companion

An interpretation of the X-ray emission in terms of accretion onto a compact companion is questionable on the above grounds. However, it is more difficult to rule out a normal

(nondegenerate) stellar companion. Such a companion is expected to be much less massive than the W-R star given that the radial velocity variations reported by Firmani et al. (1980) are of low amplitude. Arguments for binarity have recently been strengthened on the basis of long-term coherent optical variability seen in data sets spanning more than 15 years with a well-determined period P = 3.765 ± 0.0001 days (Georgiev et al. 1999). Georgiev et al. have argued that if the optical variability is due to a stellar companion then it is most likely orbiting very close to EZ CMa near the base of the wind in order to explain variations in the N V lines. We show below that a close companion could account for the hard X-ray emission detected by *XMM-Newton*.

To constrain the separation, we assume that P = 3.765 d is an orbital period and that the companion mass is much less than that of the W-R star $M_{wr} \approx 16$ $M_\odot$ (Hamann & Koesterke 1998). Kepler's third law then gives the separation in AU as $a_{AU} \approx 0.12$, or equivalently a ≈ 25 $R_\odot$. A nearly identical separation is obtained if one uses the values of $M_{wr} \approx 10$ $M_\odot$ and the companion mass $M_{comp} \approx 1.3$ $M_\odot$ adopted by Firmani et al. (1980).

We now assume that the hard X-ray component is produced by the W-R wind shocking onto the lower mass companion and that the W-R wind is dominant. In this case the contact surface is the surface of the companion star, as discussed in more detail by Luo, McCray, & MacLow (1990). Because of the close separation, radiative cooling may be important (eq. [8] of Stevens et al. 1992; eq. [52] of Usov 1992). We thus consider both adiabatic and radiative shocks. The close separation also raises the question of whether hard X-rays could escape from the overlying W-R wind and be detected. As already noted (Sec. 5.2), the radius of optical depth unity at 4 keV is $R_{\tau=1}(4\ \mathrm{keV}) \approx 0.3$ AU, so some absorption of the hard X-rays could occur. However, the absorption will depend critically on wind properties such as the clumping factor, and the actual value of $R_{\tau=1}$ in a clumped wind would be less than that given above, which is based on the assumption of a spherical, homogeneous wind. Thus, without more specific information on wind geometry and homogeneity the escape of hard X-rays (∼4 keV) from radii smaller than 0.3 AU is not precluded.

The inferred radius of the companion R_{comp} is obtained by equating the unabsorbed luminosity of the hard component (Table 3) with the predicted shock luminosity, where the predicted shock luminosity is different in the adiabatic and radiative cases (eqs. [79], [80] of Usov 1992, respectively). Using the mass loss parameters in Sec. 4.2.1 and the unabsorbed hard-component flux $F_x^{(hot)}(0.2\text{ - }10\ \mathrm{keV}) = 7.8 \times 10^{-13}$ ergs cm^{-2} s^{-1}, the adiabatic case gives $a_{AU} = 0.20 d_{kpc}^{0.25} (R_{comp}/R_\odot)^{0.75}$. For $a_{AU} = 0.12$ and the probable distance range d_{kpc} = 0.575 - 1.8 the companion radius is $R_{comp} \approx 0.4$ - 0.6 $R_\odot$. A similar calculation in the radiative case gives $R_{comp} \approx 0.12$ - 0.16 $R_\odot$. In the above, we have used the luminosity in a specific energy range (0.2 - 10 keV) as an approximation for the total X-ray luminosity

integrated over all frequencies. In general, the luminosity within a specific bandpass will be less than the value over all frequencies so the derived values of R_{comp} are in fact lower limits.

The observed temperature $kT_{hot} \approx 3.5$ [3.0 - 4.2] keV is also compatible with a shocked companion interpretation. The observed temperature derived from spectral fits is an average that includes contributions from the hottest shocked plasma at $kT_{s,max}$ along the line-of-centers and cooler plasma downstream. Thus, the observed value will in general be *less* than the maximum temperature. The difference between the observed temperature and $kT_{s,max}$ will depend on several poorly known factors including wind chemical composition and the importance of radiative cooling. As a rough estimate, one expects an observed temperature $kT \approx 0.8 kT_{s,max}$ in the adiabatic case (eq. [83] ff. of Usov 1992).

For EZ CMa, the maximum predicted temperature for an adiabatic shock in a He-dominated wind is $kT_{s,max} \approx 7.5$ keV (Sec. 5.2), assuming that the wind has reached terminal speed $v_\infty = 1700$ km s^{-1} at the shock. However, at the close separation of interest here ($a \approx 25$ $R_\odot$), the wind may not have reached terminal speed. Using the velocity profile and stellar radius $R_{wr} = 2.5$ $R_\odot$ given by Hillier (1987), we obtain $a/R_{wr} \approx 10$ and the wind is at or near terminal speed when it impacts the companion. But, using the radius $R_{wr} = 3.5$ $R_\odot$ and $\beta = 3$ wind velocity law of Schmutz (1997) then $a/R_{wr} \approx 7.1$ and the wind speed is $v_{wr} \approx 0.64$ v_∞. In this case, $kT_{s,max} \approx 3.1$ keV. Thus, based on the rough approximation that the observed temperature should be ≈ 0.8 $kT_{s,max}$, we would expect observed values in the range ≈2.5 - 6 keV. The values measured from spectral fits are well within this range.

We thus conclude that the X-ray luminosity and observed temperature of the hard component are compatible with the shocked companion hypothesis. If the companion mass is much less than that of the W-R star then the inferred companion radius is at least $R_{comp} \approx 0.2$ - 0.6 $R_\odot$. This would correspond to a main-sequence (MS) M-type star, but clearly such a low mass star could not yet have reached the MS if it formed contemporaneously with the W-R star. Thus, a pre-main-sequence (PMS) companion would seem more likely. It may be relevant here that some W-R stars such as γ^2 Vel are now believed to be associated with PMS objects (Pozzo et al. 2000; Skinner et al. 2001). If the putative companion is indeed a late-type star then interaction of the W-R wind with the companion's magnetic field would be an important factor to include in more detailed models. Our analysis shows that the observed temperature of the hot component is somewhat less than that expected for an adiabatic shock if the wind has reached terminal speed. This could be an indication that radiative cooling is important and the adiabatic approximation is breaking down at close separation, or perhaps that the W-R wind has not reached terminal speed at the shock. Radiative braking of the WR wind by the the companion star can also lead to lower X-ray temperatures than predicted by simple models (Gayley, Owocki, & Cranmer 1997) but this

effect would be of little importance for a lower mass companion that is less luminous than the WR star.

6. Summary

Overall, the X-ray properties derived for EZ CMa using new *XMM-Newton* data are in good agreement with previous *ASCA* results (Skinner et al. 1997). The improved signal-to-noise in *XMM-Newton* spectra yields more accurate measurements of the X-ray absorption and plasma temperatures. The temperature of the dominant cool component is identical to that obtained with *ASCA*, but the hot component temperature is revised upward by ≈35% to $kT_{hot} \approx 3.5$ [3.0 - 4.2] keV.

The origin of the hotter plasma remains obscure, but neutron star accretion models are difficult to justify based on X-ray luminosity considerations and the close similarity between the X-ray and radio properties of EZ CMa and WR 110, where the latter is *not* a candidate WR + c system. We have argued that the hard X-rays could from the W-R wind shocking onto a normal low-mass stellar companion, but direct evidence for such a companion is still lacking. Also, the failure to detect periodic X-ray variability with *ROSAT* is somewhat difficult to reconcile with a companion interpretation unless the orbital elements are not conducive to X-ray variability, as for example in a low eccentricity orbit. Further broad-band searches for modulated X-ray emission might be worthwhile since *ROSAT* was not sensitive to emission above 2.5 keV. The *XMM-Newton* spectra show that about one-third of the observed flux emerges above 2.5 keV (Table 3) and essentially all of this is due to the hard component.

Until conclusive evidence for binarity is found, alternative models that are capable of producing hard X-rays in the absence of a companion should be explored. Of particular interest are models that incorporate wind - magnetic field interactions since it has been proposed that the variability of EZ CMa may be due to corotating structures at or near the surface (St.-Louis et al. 1995). Possible evidence for magnetic activity in the form of short-duration (∼1 hr) optical variability has also been reported (Duijsens et al. 1996).

The *XMM-Newton* spectra also reveal two interesting anomalies that deserve further study. First, the absorption column density derived from *XMM-Newton* spectra (Table 3) is comparable to *Einstein* and *ASCA* values and leads to an estimate of $A_v = 1.8$ [1.5 - 2.0] that is at least twice as large as previous optical/UV determinations. This suggests that excess X-ray absorption could be present that is not seen in the optical/UV, possibly due to the surrounding ring nebula, or perhaps that A_v is slightly underestimated from

optical/UV studies. Second, the *XMM-Newton* spectra indicate that WN abundances may be substantially different than assumed in earlier work. In particular, all spectral models examined here give a best-fit Fe abundance that is a factor of ∼4 below the reference value for WN stars given in VCW86, and a similar depletion is noted when using cosmic abundances (AG89) as a reference. Some caution is advised since the low Fe abundance was inferred from moderate resolution CCD spectra where line blending is present, but the repeatibility of this result across several different types of models does suggest that the underabundance is real.

Finally, the close similarities between EZ CMa and WR 110 apparent in Table 4 and Figure 8 represent a first step toward a unified observational picture of X-ray and radio emission in WN stars. These close similarities provide strong evidence that the physical mechanisms responsible for the X-ray and radio continuum emission in these two WN stars are identical, even though their optical properties are obviously different. If an unseen companion is responsible for the optical variability and hard X-ray emission in EZ CMa then the similarities in Table 4 implicate an unseen companion in WR 110 as well. The properties of such a companion were derived in our previous analysis of WR 110 (SZGS02) but are not as tightly constrained as for EZ CMa since WR 110 has no known regular optical variability on which to base an estimate of the orbital period. Other W-R stars which have so far shown no direct evidence for binarity but which could also harbor unseen companions are those with prominent X-ray emission such as the WN4 star WR1 (HD 4004).

This work was supported by NASA grant NAG5-10325. Research at PSI has been supported by the Swiss National Science Foundation under grant 2100-049343. This work was based on observations obtained with XMM-Newton, an ESA science mission with instruments and contributions directly funded by ESA member states and the USA (NASA). We thank members of the XMM-Newton, VLA, and HEASARC (NASA/GSFC) support teams for their assistance. This research has made use of the SIMBAD astronomical database operated by CDS at Strasbourg, France.

Table 1. XMM-Newton Observations of EZ CMa[a]

Parameter	Value
Start (UT)	29 Oct 2001 21:35
Stop (UT)	30 Oct 2001 00:57
Exposure (ksec)	9.5 (PN), 12.1 (per MOS)
Count Rate $\pm 1\sigma$ (c s^{-1})	0.26 ± 0.03 (PN), 0.12 ± 0.02 (per MOS)
Flux (10^{-12} ergs cm^{-2} s^{-1})	0.97 (2.90)

[a]Count rate and standard deviation are from light curves binned at 256 s intervals. Flux is the observed value in the 0.2 - 10 keV range followed in parentheses by the unabsorbed value.

Table 2. VLA Observations of EZ CMa[a]

Frequency (GHz)	Beam FWHM (arcsec)	Duration (min.)	RMS Noise (μJy/beam)	Peak Flux (mJy/beam)	Total Flux (mJy)
1.42	6.1×4.2	23	56[b]	0.56	0.57
4.86	1.7×1.1	20	39	1.01	1.02
8.44	0.9×0.7	20	29	1.60	1.74
14.94	0.5×0.4	31	99	2.31	2.38
22.46	0.4×0.3	30	150	3.16	3.15

[a]All data were obtained in BnA configuration on 1999 Oct 19 from 1024 - 1341 UT. Observations were obtained at each frequency in two orthogonal polarization channels, each with a bandwidth of 50 MHz. Fluxes and beam sizes are from cleaned Stokes I maps. Primary flux calibrator was 3C286. The radio position of EZ CMa measured from 8.44 GHz maps is RA(2000) = 06 h 54 m 13.045 s, DEC(2000) = -23° $55'$ $41.94''$.

[b]The RMS noise at 1.42 GHz is larger than predicted by sensitivity calculations due to the presence of other bright sources in the field.

Table 3. X-ray Spectral Properties of EZ CMa[a]

Parameter	Value
N_H (10^{21} cm^{-2})	4.0 [3.4 - 4.4]
kT_{cool} (keV)	0.59 [0.55 - 0.63]
kT_{hot} (keV)	3.5 [3.0 - 4.2]
$norm_{cool}$	3.41×10^{-5}
$norm_{hot}$	1.04×10^{-5}
EM_{cool}/EM_{hot}	3.3
Abundances	varied
χ^2/dof	234.5/217
F_x(0.2 - 10 keV)[b]	0.97 (2.90)
F_x(2.5 - 10 keV)[b]	0.31 (0.33)
$F_x^{(hot)}$(0.2 - 10 keV)[b]	0.49 (0.78)

[a]X-ray properties are from simultaneous fits of PN, MOS1, and MOS2 spectra using an absorbed 2T optically thin plasma model (2T VAPEC). Brackets enclose 90% confidence intervals. Abundances were initialized to the WN values given in Table 1 of VCW86 (renormalized to H = 1.0 in XSPEC) and N, Ne, Mg, Si, S, Fe abundances were then varied to obtain the best fit. Iron converges to an abundance Fe = 0.23 [0.15 - 0.32]. The emission measure for a He-dominated plasma is EM = $1.9 \times 10^{59} d_{kpc}^2 norm$ cm^{-3}. The X-ray position obtained by averaging the results of all three EPIC cameras is RA(2000) = $06^h\ 54^m\ 13.07^s$, DEC(2000) = $-23^\circ\ 55'\ 41.5''$.

[b]Fluxes are the observed (absorbed) values followed in parentheses by the unabsorbed values in units of 10^{-12} ergs cm^{-2} s^{-1}.

Table 4. Comparison of EZ CMa (WR 6) and WR 110

Parameter	EZ CMa	WR 110
Spectral type[a]	WN4	WN5-6
Distance (kpc)[a]	0.58 - 1.8	1.28
Radio spectral index (α)	$+0.69 \pm 0.05$	$+0.64 \pm 0.10$
$\dot{M}$ (10^{-5} $M_\odot$ yr^{-1})	3.5 (1.2 - 6.5)[b]	4.9
N_H (10^{22} cm^{-2})	0.4 ± 0.05	1.05 ± 0.16
kT_{cool} (keV)	0.59 ± 0.04	0.55 ± 0.07
kT_{hot} (keV)	3.5 ± 0.6	≥ 3
L_x (10^{32} ergs s^{-1})	5.0 (1.1 - 11.2)[b]	4.4
L_x/L_{wind}	$\sim 10^{-5}$	$\sim 10^{-5}$
L_{6cm}/L_x (10^{-15} Hz^{-1})	3.6	5.2

[a]Spectral types and the distance for WR 110 are from vdH01. The smaller distance for EZ CMa is from *Hipparcos* and the larger is from Howarth & Schmutz 1995. The X-ray properties of WR 110 are from SZGS02 except that L_x is quoted here in the 0.2 - 10 keV range.

[b]The quoted value is for an intermediate distance of 1.2 kpc, followed in parentheses by the range of values corresponding to d = 0.58 - 1.8 kpc. L_x is the unabsorbed luminosity in the 0.2 - 10 keV range.

REFERENCES

[]Abbott, D.C., Bieging, J.H., Churchwell, E., & Torres, A.V. 1986, ApJ, 303, 239

[]Altenhoff, W.J., Thum, C., & Wendker, H.J., 1994, A&A, 281, 161

[]Anders, E., & Grevesse, N. 1989, Geochim. Cosmochim. Acta, 53, 197 (AG89)

[]Arnaud, K.A. 1996, in Astronomical Data Analysis Software and Systems V, eds. G. Jacoby & J. Barnes, (San Francisco: ASP), 101, 17

[]Baum, E., Hamann, W.-R., Koesterke, L. & Wessolowski, U. 1992, A&A, 266, 402

[]Cassinelli, J.P., Miller, N.A., Waldron, W.A., MacFarlane, J.J., & Cohen, D.H., 2001, ApJ, 554, L55

[]Cherepashchuk, A.M. 1976, Soviet Astr. Letters, 2, 138

[]Cohen, D. et al. 2002, ApJ, in prep.

[]Contreras, M.E. & Rodriguez, L.F. 2000, Rev. Mex. de Astron. y Astrof., 36, 135

[]Davidson, K. & Ostriker, J.P., 1973, ApJ, 179, 585

[]Duijsens, M.F.J., van der Hucht, K.A., van Genderen, A.M., Schwarz, H.E., Linders, H.P.J., & Kolkman, O.M. 1996, A&AS, 119, 37

[]Dumm, T. et al. 2002, to appear in New Visions of the X-ray Universe in the XMM-Newton and Chandra Era, ed. F. Jansen, ESA SP-488, in press

[]Feldmeier, A., Kudritzki. R.-P., Palsa, R. Pauldrach, A.W.A., & Puls, J., 1997, A&A, 320, 899

[]Firmani, C., Koenigsberger, G., Bisiacchi, G.F., Moffat, A.F.J., & Isserstedt, J. 1980, ApJ, 239, 607

[]Gayley, K.G. & Owocki, S.P., 1995, ApJ, 446, 801

[]Gayley, K.G., Owocki, S.P., & Cranmer, S.R., 1997, ApJ, 475, 786

[]Georgiev, L.N., Koenigsberger, G., Ivanov, M.M., St.-Louis, N., & Cardona, O. 1999, A&A, 347, 583

[]Gorenstein, P. 1975, ApJ, 198, 95

[]Hamann, W.-R. & Koesterke, L. 1998, A&A, 333, 251

[]Harries, T.J., Howarth, I.D., Schulte-Ladbeck, R.E., & Hillier, D.J. 1999, MNRAS, 302, 499

[]Hillier, D.J., 1987, ApJS, 63, 965

[]Hillier, D.J., Kudritzki, R.P., Pauldrach, A.W., Baade, D., Cassinelli, J.P., Puls, J., & Schmitt, J.H.M.M., 1993, A&A, 276, 117

[]Hogg, D.E. 1989, AJ, 98, 282

[]Howarth, I.D. & Schmutz, W. 1995, A&A, 294, 529

[]Ignace, R., Oskinova, L.M., & Foullon, C., 2000, MNRAS, 318, 214

[]Jansen, F. et al., 2001, A&A, 365, L1

[]Kahn, S.M. et al., 2001, A&A, 365, L312

[]Lamontagne, R., Moffat, A.F.J., & Lamarre, A. 1986, AJ, 91, 925

[]Leitherer, C. & Robert, C. 1991, ApJ, 377, 629

[]Lemen, J.R., Mewe, R., Schrijver, C.J., & Fludra, A., 1989, ApJ, 341, 484

[]Lucy, L.B., 1982, ApJ, 255, 286

[]Lucy, L.B. & White, R.L., 1980, ApJ, 241, 300

[]Luo, D., McCray, R., & MacLow, M-M., 1990, ApJ, 362, 267

[]MacFarlane, J.J. et al. 1991, ApJ, 380, 564

[]Moffat, A.F.J., Firmani, C., McLean, I.S., & Seggewiss, W. 1982, in Wolf-Rayet Stars: Observations, Physics, Evolution, eds. C. de Loore & A. Willis (Dordrecht: Reidel), 577

[]Morrison, R. & McCammon, D. 1983, ApJ, 270, 119

[]Owocki, S.P., Castor, J.I., & Rybicki, G.B., 1988, ApJ, 335, 914

[]Owocki, S.P. & Cohen, D.H. 2001, ApJ, 559, 1108

[]Perryman, M.A.C. et al. 1997, A&A, 323, 49

[]Pozzo, M., Jeffries, R.D., Naylor, T., Totten, E.J., Harmer, S., & Kenyon, M. 2000, MNRAS, 313, L23

[]Prilutskii, O., Usov, V.V., 1976, SvA-AJ, 20,2

[]Prinja, R.K., Barlow, M.J., & Howarth, I.D., 1990, ApJ, 361, 607

[]Runacres, M.C. & Owocki, S.P., 2002, A&A, 381, 1015

[]Schmutz, W. 1997, A&A, 321, 268

[]Skinner, S.L., Güdel, M., Schmutz, W., & Stevens, I.R., 2001, ApJ, 558, L113

[]Skinner, S.L., Itoh, M., & Nagase, F. 1997, New Astron., 3, 37

[]Skinner, S.L., Zhekov, S., Güdel, M., & Schmutz, W. 2002, ApJ, 572, in press (SZGS02)

[]Stevens, I.R. & Willis, A.J. 1988, MNRAS, 234, 783

[]St.-Louis, N., Dalton, M.J., Marchenko, S.V., Moffat, A.F.J., & Willis, A.J., 1995, ApJ, 452, L57

[]Strüder, L. et al., 2001, A&A, 365, L18

[]Turner, M.J.L. et al., 2001, A&A, 365, L27

[]Usov, V.V. 1992, ApJ, 389, 635

[]van der Hucht, K.A., 2001, New Ast. Rev., 45, 135 (vdH01)

[]van der Hucht, K.A., Cassinelli, J.P., & Williams, P.M., 1986, A&A, 168, 111 (VCW86)

[]Waldron, W. & Cassinelli, J.P., 2001, ApJ, 548, L45

[]White, R.L. & Long, K.S., 1986, ApJ, 310, 832

[]Willis, A.J. 1996, Ap&SS, 237, 145

[]Willis, A.J. & Stevens, I.R., 1996, A&A, 310, 577 (WS96)

[]Wright, A.E. & Barlow, M.J., 1975, MNRAS, 170, 41

Fig. 1.— Smoothed X-ray contour images of the region near EZ CMa (arrow) obtained by combining data from the MOS1 and MOS2 detectors. The combined exposure time is ≈24.2 ksec and coordinate overlay is J2000. The respective energy bands, total EZ CMa source counts (MOS1 + MOS2) after background subtraction, and S/N ratio in each image are: *left:* broad-band (0.3 - 10 keV), 2933 counts, S/N = 52.1; *right:* hard-band (5 - 10 keV), 44 counts, S/N = 6.0.

Fig. 2.— Background-subtracted EPIC-MOS light curves of EZ CMa in the 0.3 - 8.0 keV range. Error bars are 1σ and the binsize is 512 s. The average count rate is 0.12 ± 0.02 c s^{-1} per MOS.

Fig. 3.— Histogram plot of the background-subtracted EPIC-PN spectrum of EZ CMa rebinned to a minimum of 15 counts per bin for display.

Fig. 4.— Best fit 2T VAPEC model using the parameters in Table 3 overlaid on the MOS1 spectrum. The spectrum is rebinned to a minimum of 20 counts per bin. Residuals are in the sense of data - model.

Fig. 5.— Contributions of the cool and hot components to the best-fit 2T VAPEC model of the MOS-1 spectrum. The hot component dominates the emission above ≈2.5 keV.

Fig. 6.— Differential emission measure (DEM) model of EZ CMa based on a simultaneous fit of the EPIC spectra from all three detectors using an absorbed Chebyshev polynomial model (C6PVMKL). The best-fit column density is $N_H = 4 \times 10^{21}$ cm^{-2} and abundances were allowed to vary relative to the canonical WN abundances given by VCW86.

Fig. 7.— The radio spectral energy distribution of EZ CMa based on total fluxes given in Table 1. Error bars are the formal errors in total flux computed by the Gaussian fit AIPS task IMFIT. The solid line is a best-fit power-law model, which gives a spectral index $\alpha = +0.69 \pm 0.05$ (90% confidence limits).

Fig. 8.— A comparison of the PN spectra of EZ CMa and WR110. Spectra are rebinned to a minimum of 20 counts per bin.

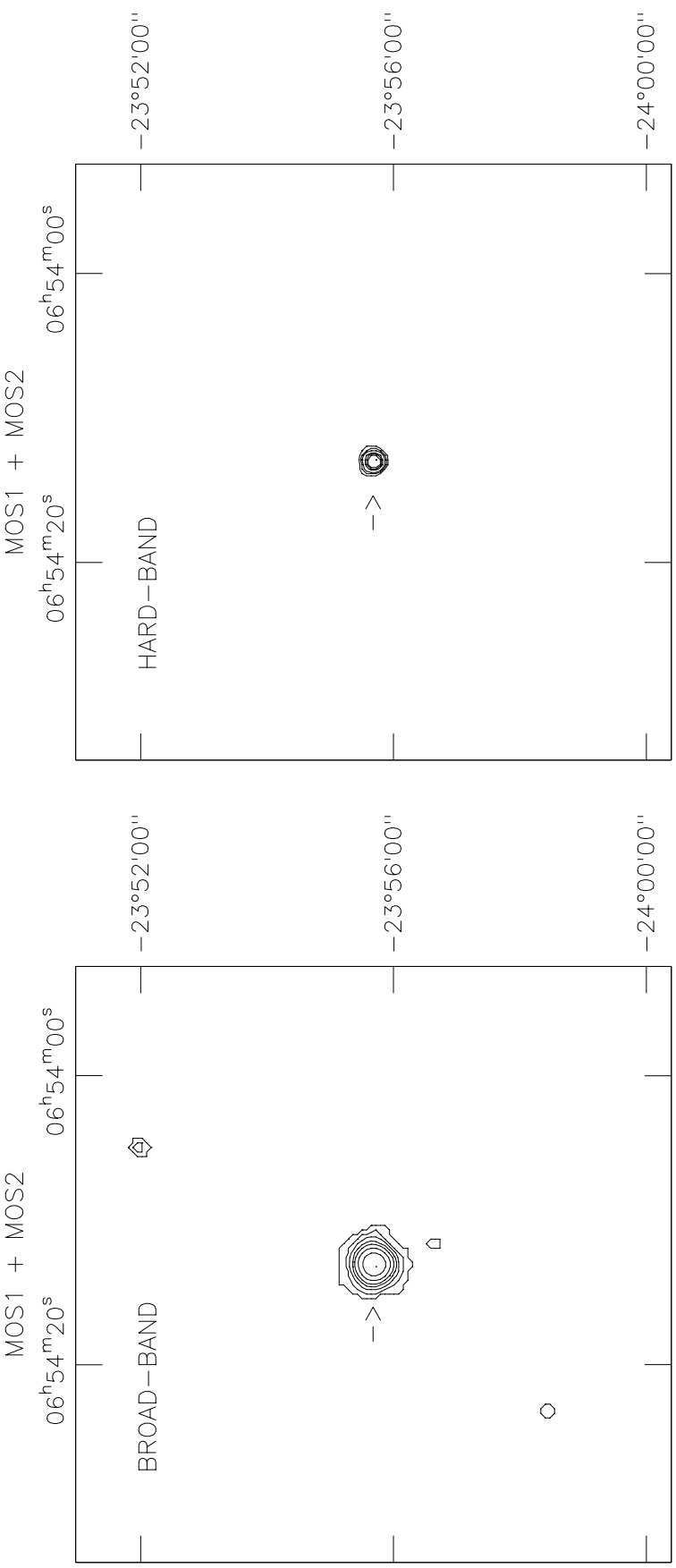
MOS1 + MOS2
HARD−BAND
BROAD−BAND
06h54m20s
06h54m00s
−23°52'00''
−23°56'00''
−24°00'00''

Fig. 1.—

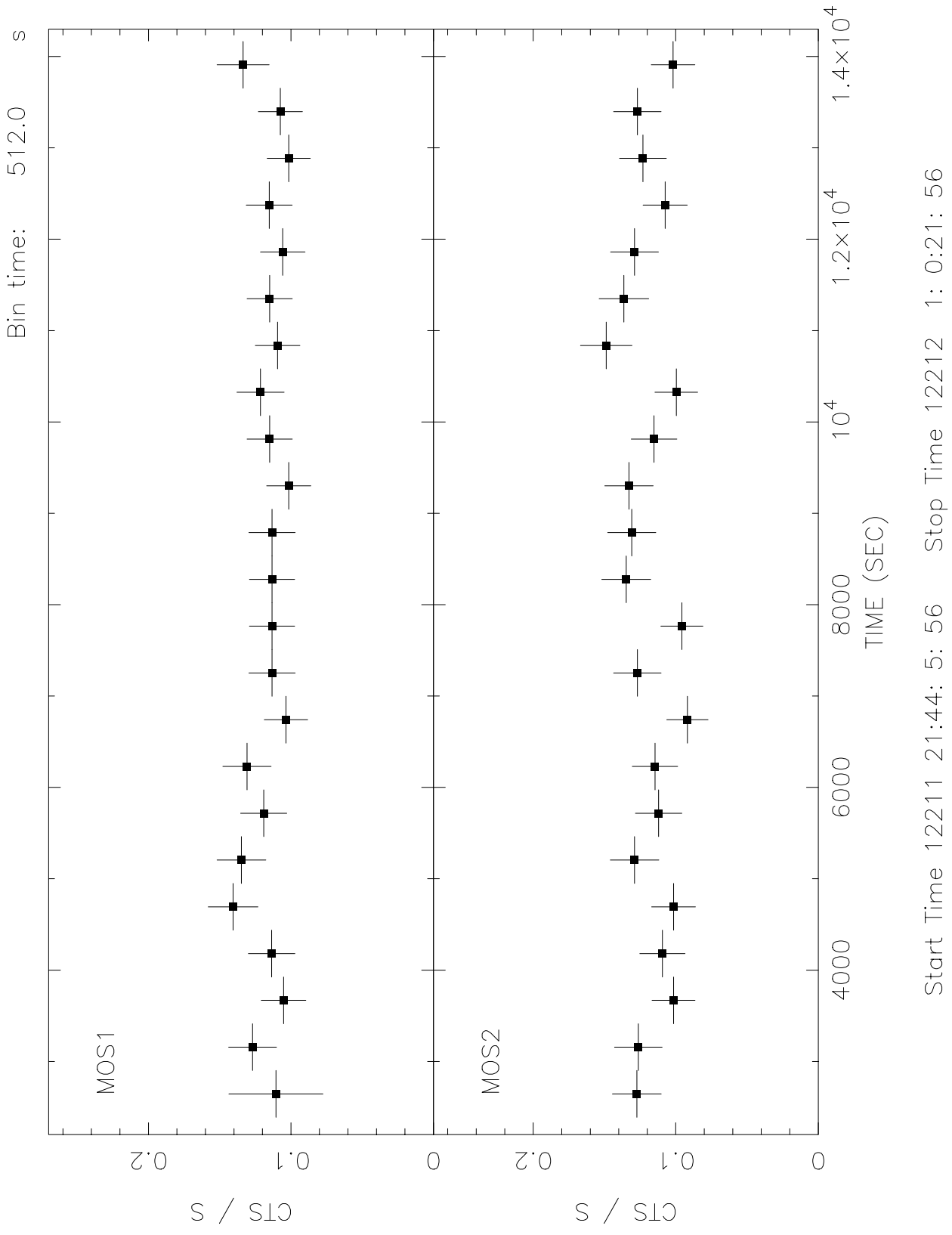
Bin time: 512.0 s
MOS1
MOS2
CTS / S
0
0.1
0.2
4000
6000
8000
10^4
1.2×10^4
1.4×10^4
TIME (SEC)
Start Time 12211 21:44: 5: 56
Stop Time 12212 1: 0:21: 56

Fig. 2.—

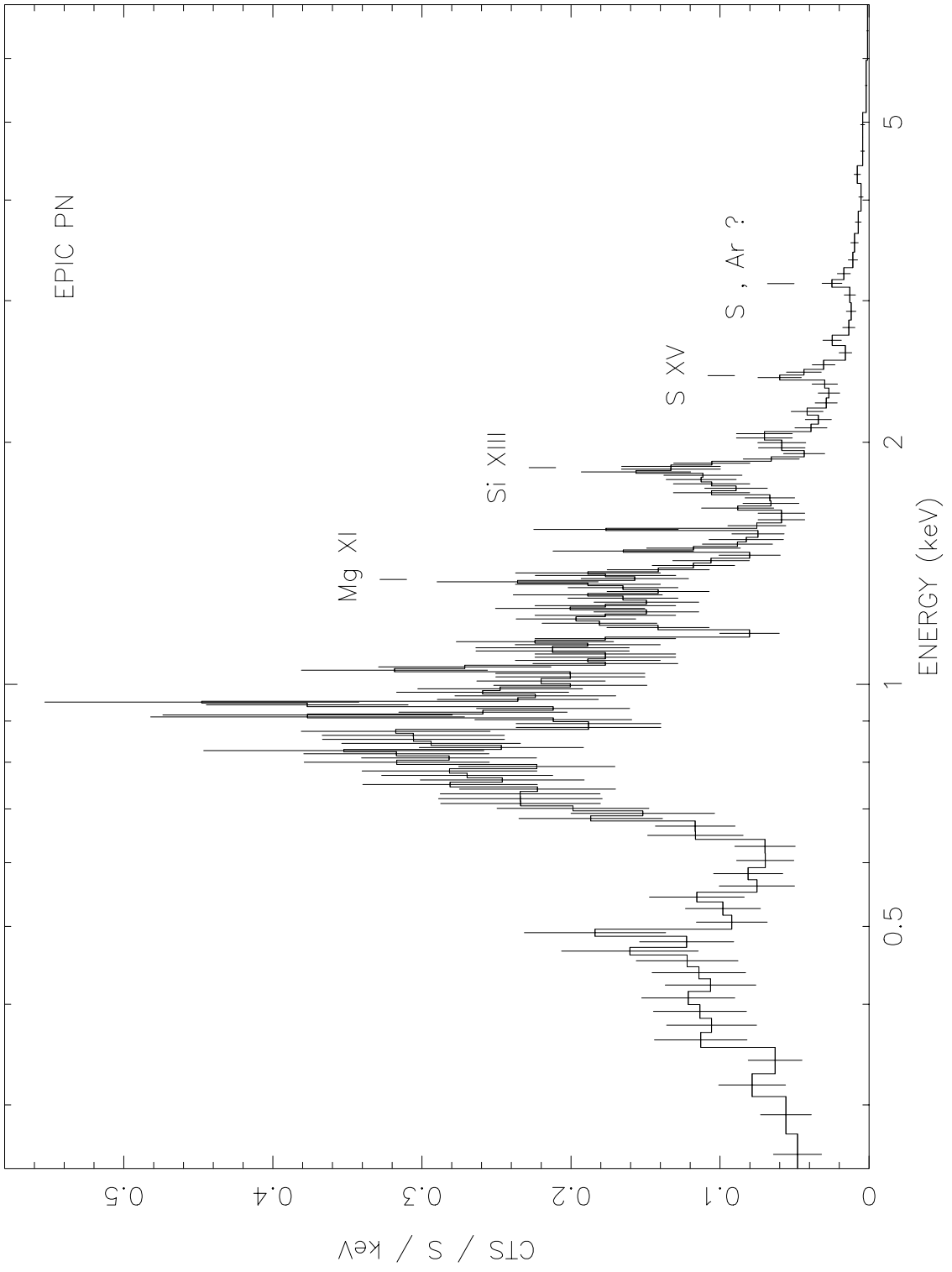
EPIC PN
Mg XI
Si XIII
S XV
S , Ar ?
CTS / S / keV
ENERGY (keV)
0
0.1
0.2
0.3
0.4
0.5
1
2
5

Fig. 3.—

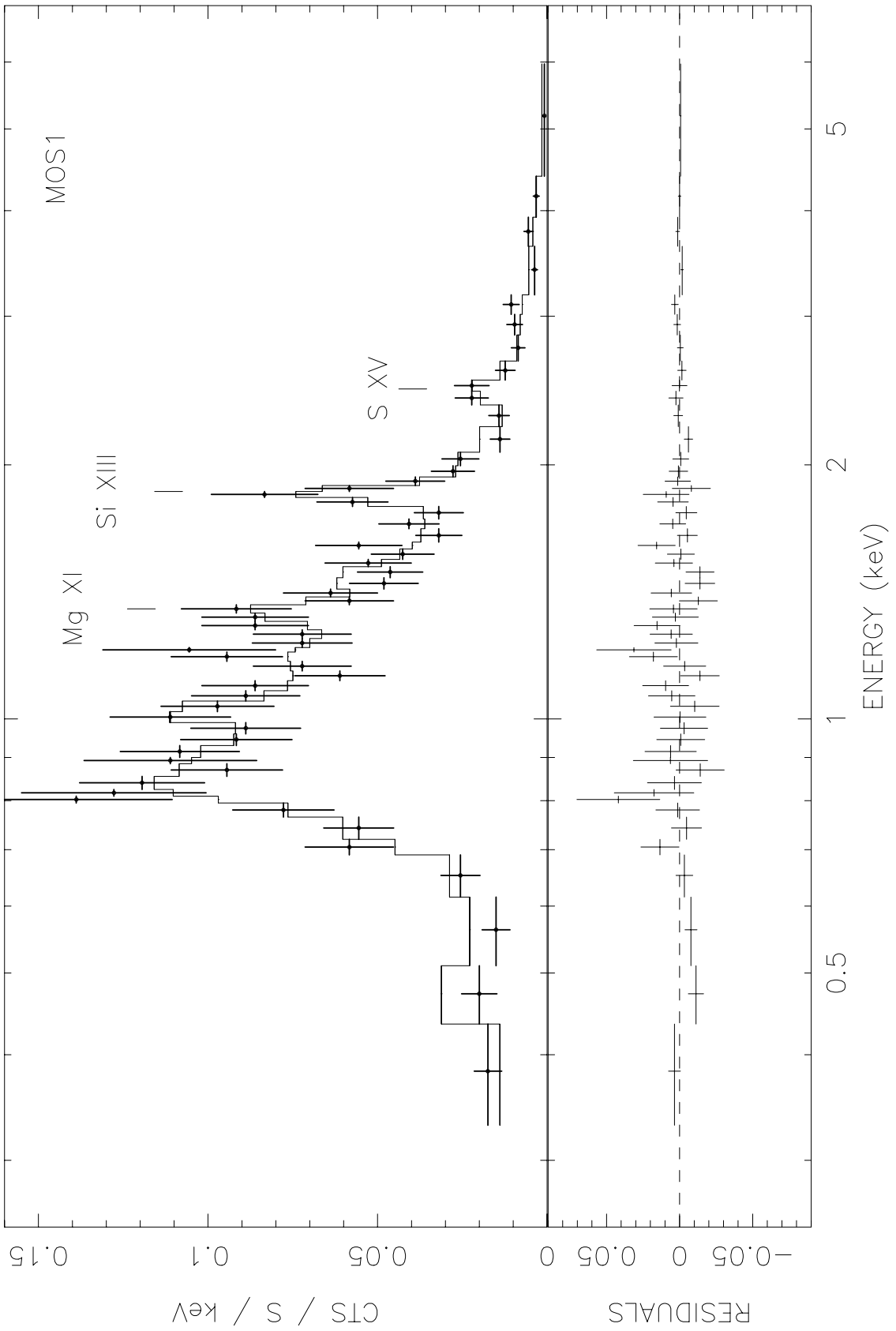
MOS1
Mg XI
Si XIII
S XV
CTS / S / keV
RESIDUALS
ENERGY (keV)
0.15
0.1
0.05
0
−0.05
0.5
1
2
5

Fig. 4.—

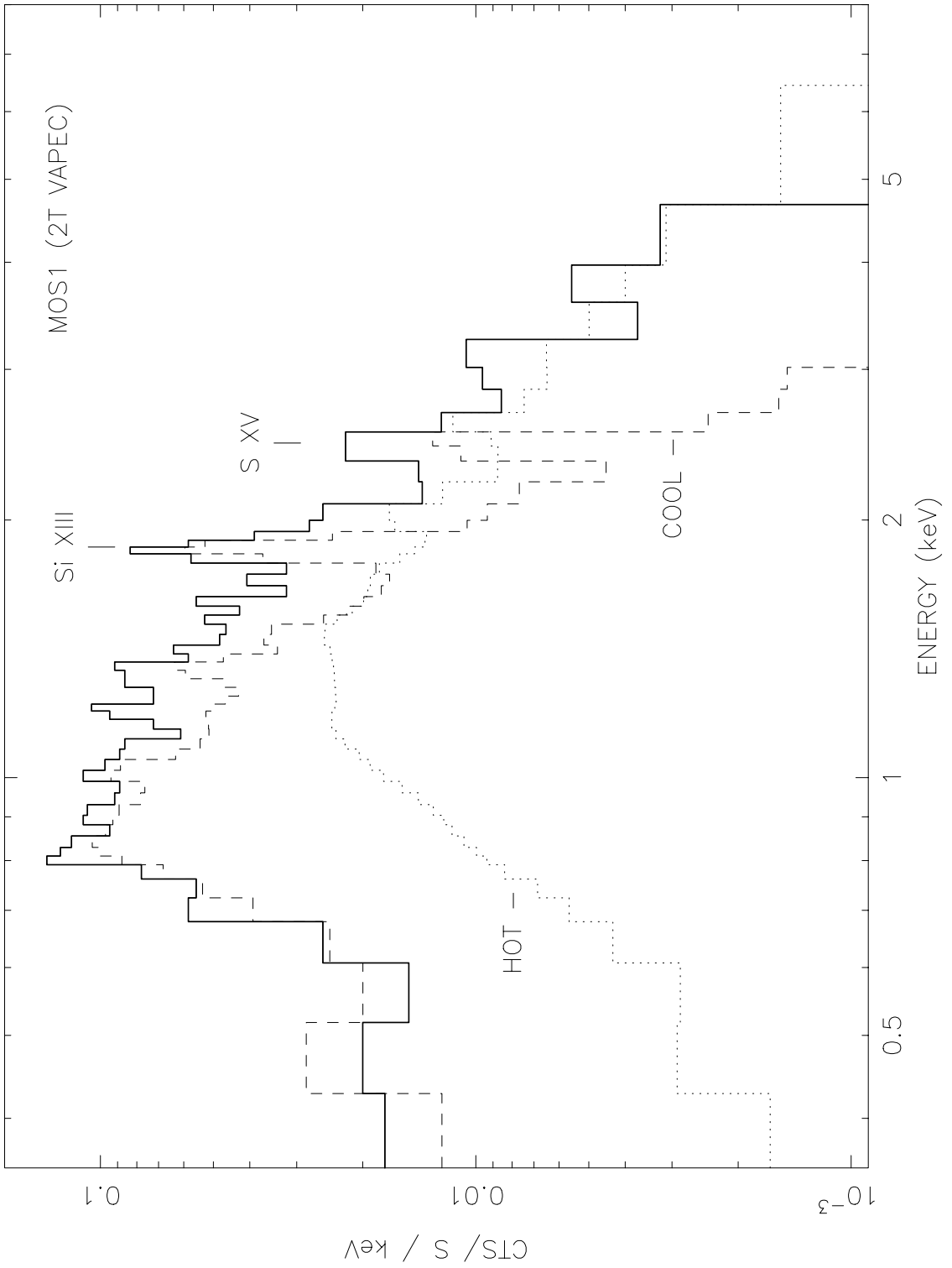
MOS1 (2T VAPEC)
Si XIII
S XV
COOL
HOT
ENERGY (keV)
0.5
1
2
5
0.1
0.01
10^-3
CTS/ S / keV

Fig. 5.—

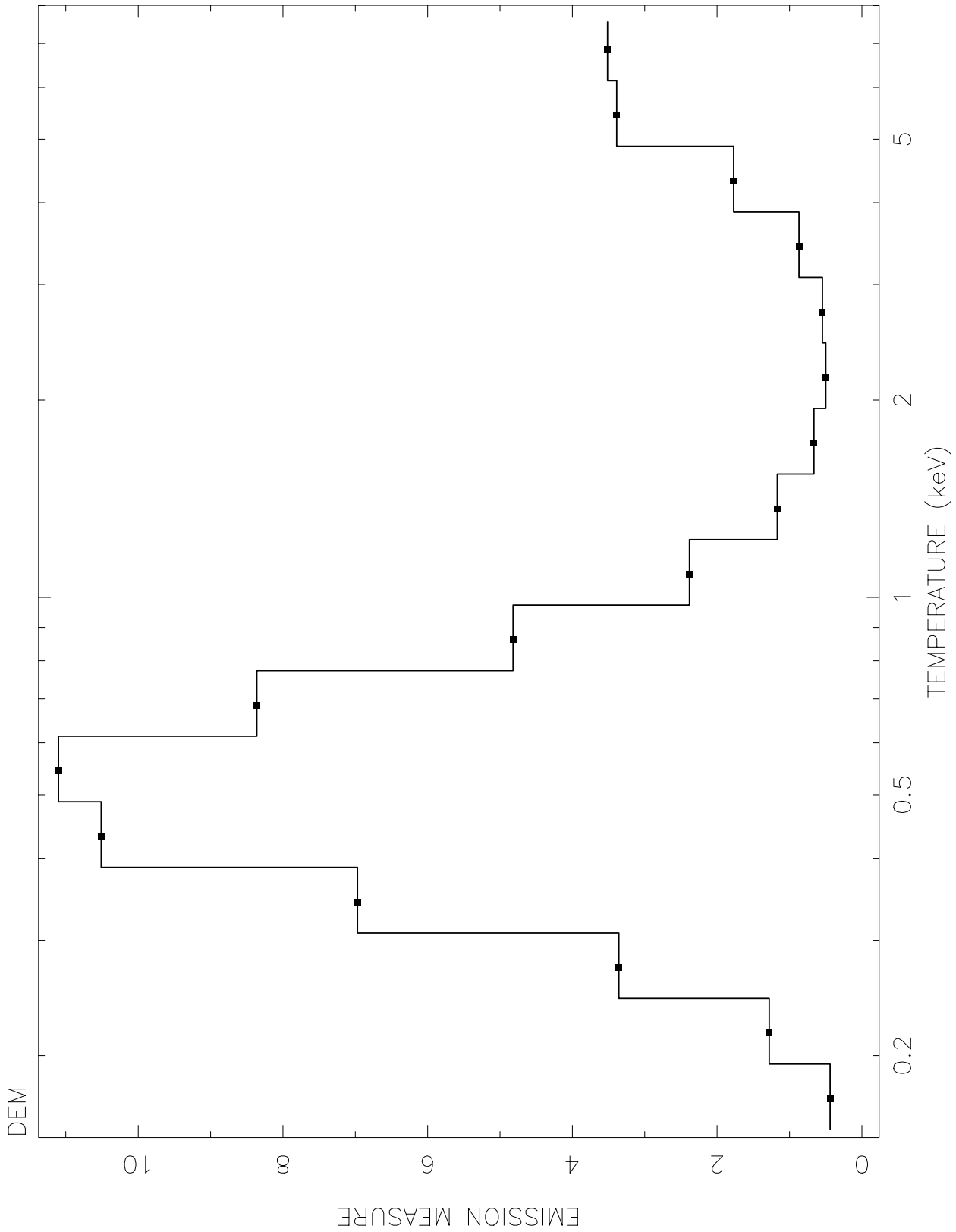

Fig. 6.—

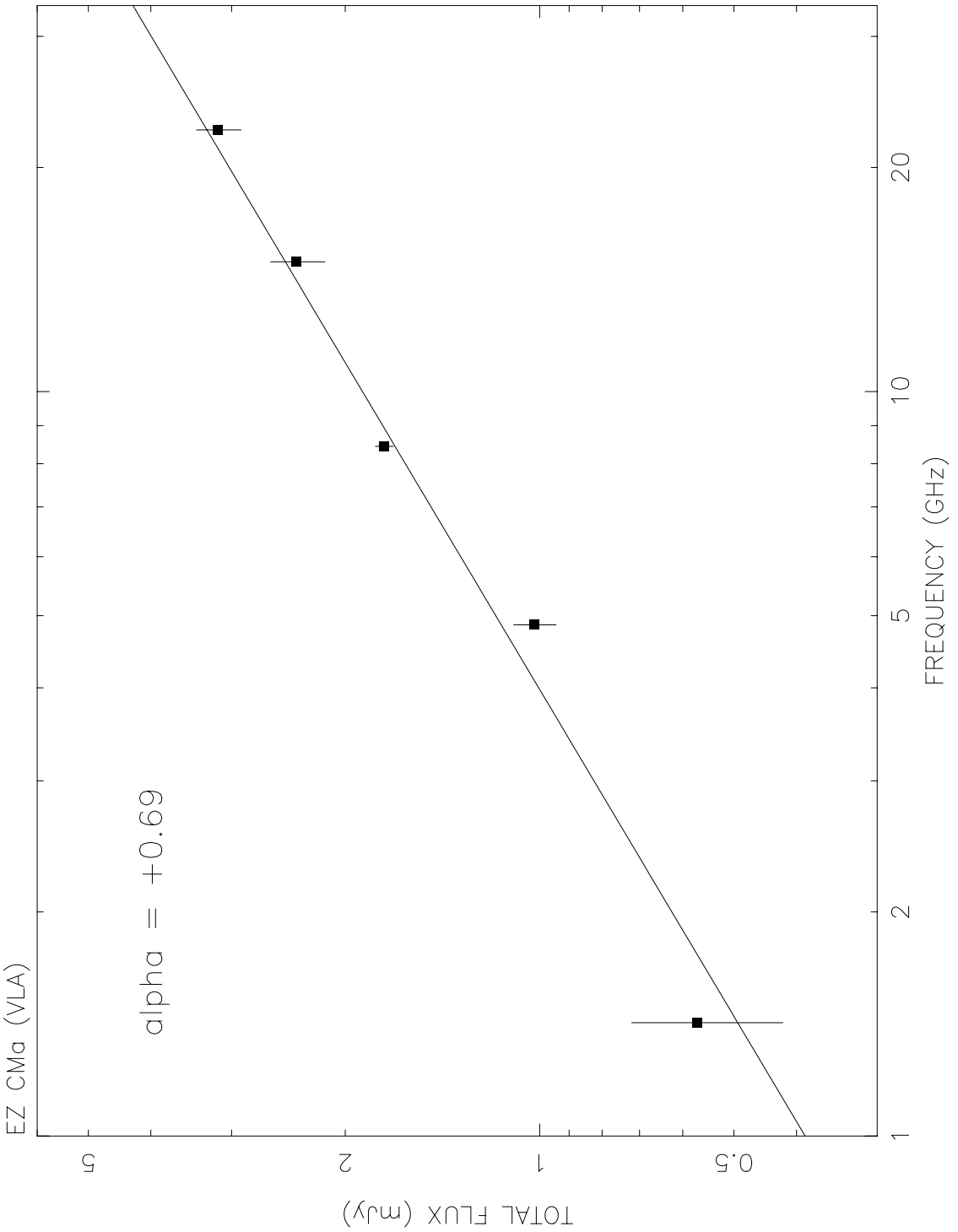
EZ CMa (VLA)
alpha = +0.69
TOTAL FLUX (mJy)
FREQUENCY (GHz)
0.5
1
2
5
1
2
5
10
20

Fig. 7.—

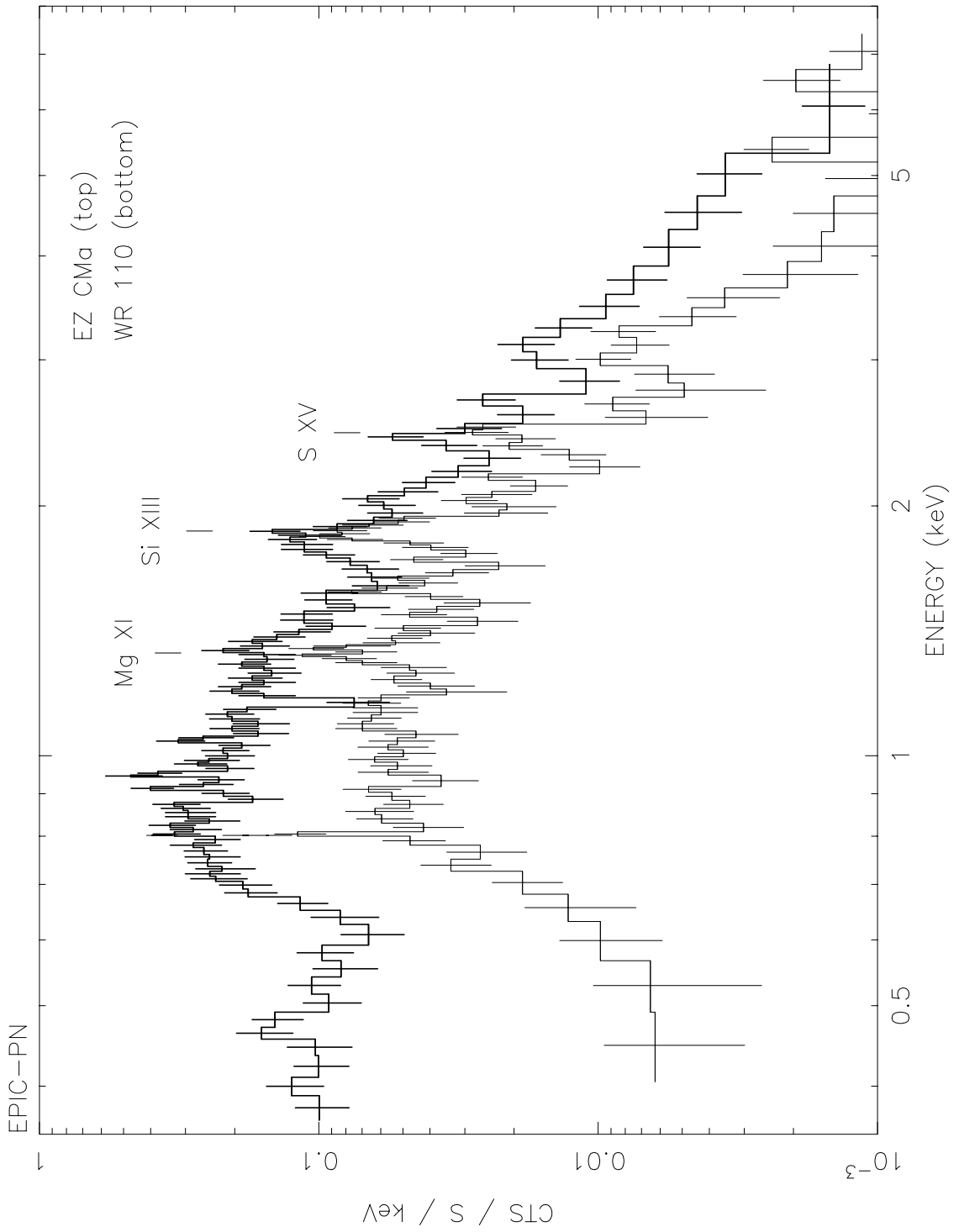
EZ CMa (top)
WR 110 (bottom)
Mg XI
Si XIII
S XV
EPIC–PN
CTS / S / keV
ENERGY (keV)
1
0.1
0.01
10^-3
0.5
1
2
5

Fig. 8.—